Image-based river discharge estimation by merging heterogeneous data with information entropy theory

Nour Chahrour, William Castaings, Eric Barthélemy

Image-based river discharge estimation by merging heterogeneous data with information entropy theory.

Chahrour Nour[a,b], Castaings William[b], Barthélemy Eric[c,*]

[a] Univ. Grenoble Alpes, CNRS, INRAE, 38000 Grenoble, France
[b] TENEVIA, 38240 Meylan, France
[c] Univ. Grenoble Alpes, CNRS, Grenoble INP, LEGI, 38000 Grenoble, France

Abstract

An information entropy based approach for the discharge measurements is evaluated for the gaging of the Isère river at the Grenoble university campus. Over a four month period, six discharge measurements were made using a vessel-mounted aDcp. Simultaneously, particle tracking velocimetry (PTV) from video images was used to estimate surface velocities. The surface velocities are projected along the regularly surveyed river section of the Isère-Campus gaging station. The vertical velocity profile at each stream-wise location is approximated by a 1D entropy profile. Information entropy 1D velocity vertical profile depends on two parameters which are fitted using aDcp and surface velocity measurements. The inclusion of the surface velocities reduces the dispersion of the estimated entropy parameters. The measurements show that the two parameters are linearly related with a slope that is stage dependent and thus, surface velocity dependent. From there, the information entropy theory for 1D velocity distribution offers a protocol by which surface velocities only are used to compute the discharges. The protocol is calibrated with both aDcp and surface velocity measurements. It is finally validated with several events during which only surface velocities are measured. For the high water flood event the estimated discharge falls within 2% of the one estimated with the rating curve of the gaging station.

Keywords: river, discharge, surface velocity, video, information entropy, gaging curve, aDcp

1. Introduction

Discharge measurements in natural streams and rivers are of fundamental interest for hydrology and water resources management. Estimating river discharges is therefore paramount for flood mitigation, predicting hydro-electrical production, urban planning, hydraulic structure design, the calibration of hydrological models and many other water related issues.

The discharge or flow Q is the volume of water crossing the flow area per unit time and no instrument measures it directly. Because it is the flux of the water, traditional approaches to discharge evaluations break down to the estimation of the stream wise water velocity distribution across the river flow area. This distribution is surveyed at specific locations along selected

*Corresponding author
Email addresses: nour.chahrour@grenoble-inp.fr (Chahrour Nour), william.castaings@tenevia.com (Castaings William), eric.barthelemy@grenoble-inp.fr (Barthélemy Eric)

verticals. Pairs of adjacent verticals define panels of the cross-section spanning the entire water column. An elementary discharge through each panel can be estimated. Methods differ on how a velocity is assigned to the panel. For measurements using flow meters with propellers the panels can span the entire water column while with surface aDcp's (acoustic Doppler current profilers) parts of the panels close to the free surface and the bottom are not surveyed. These parts are known as blanking zones. The uncertainties of this type of panel method are discussed by Le Coz et al. (2012).

Rating curve techniques measure a flow variable, usually at a low cost, such as the free surface elevation or the free surface slope (Rantz, 1982; Manfreda et al., 2020). They are said to be continuous in the sense that these instruments can be set up to measure all the time at given sampling frequency as long as the data storage capacity allows for it. However, these continuous methods require calibration. They imply gaging the river discharge now and then to provide a correspondence between Q and the flow variable that is measured. This correspondence takes the form of a so-called rating curve. Discharge gaging techniques such as an aDcp can be sensitive to the presence of sediment load (suspended or bed load) but also dangerous and impossible to deploy during floods. For all these reasons, alternative methods have been developed for decades such as video imaging or radar probing of free surface water velocities.

Video image-based methods are extensions of conventional PIV (Particle Image Velocimetry) which has been used for many decades in experimental fluid dynamics. Using the same principles based on the analysis of the cross-correlation of image patterns, the extension and adaptation to large scale flows (LSPIV) was pioneered by Fujita and Komura (1994). This technique became widely used in river hydrometry for the measurement of surface velocities and the estimation of discharge (Fujita, 1997; Creutin et al., 2003; Muste et al., 2008; Le Coz et al., 2010). In order to reduce the impact of the heterogeneity and variability of surface textures, the influence of lighting conditions and shooting angle, variants such as Particle Tracking Velocimetry (PTV) and Space–time Image Velocimetry (STIV) were developed or adapted. While PTV is based on the detection and tracking of individual particles using cross-correlation, optical flow or other techniques (Tauro et al., 2019; Perks, 2020), STIV stacks image frames along a few search lines in the flow direction and searches for gradients in the resulting space-time image (Fujita et al., 2007, 2019). In practice many motion estimation methods used in computer vision can be used.

Discharge estimations from surface video based velocities require at least two extra pieces of information. Firstly, since all these methods provide surface velocities measurements, some assumptions need to be invoked to transform these surface velocities in vertically averaged velocities. The velocity index k_v is as straightforward way of linking a surface velocity to a vertical average velocity. Secondly, the other piece of information required is the bathymetry/water depth cross wise distribution necessary to compute a volume flux through the water column.

The idea of the velocity index goes back to (De Prony, 1804; Dulos, 1877, p. 73) and continues to be a subject of applied research (Gunawan et al., 2012; Moramarco et al., 2017; Kästner et al., 2018). The flow shallowness of large rivers (top width much larger than the depth) is expected to shape velocity distributions to be two-dimensional, and the velocity vertical profile is deemed to follow amongst others the classical logarithmic law or Prandtl's seventh power law over the water depth (Cheng, 2007). In the latter case, the theoretical velocity index for the seventh power law is $k_v = 0.875$. The value of the velocity index depends on the shape of the vertical velocity profile which is a signature of the boundary layer vertical structure. This velocity index also depends on how close from the banks the vertical is. Indeed, the velocity distribution is strongly influenced by bank induced friction (Mueller, 2013) and secondary currents. The boundary layer is affected by the turbulence of the flow which depends on the flow aspect ratio, on the bed-roughness, on bed forms, the Froude and the Reynolds numbers.

Assumptions on the velocity vertical profile are also used in aDcp commercial softwares to complement the vertical profile in the blanking zones near the free surface and the bottom. The log-profile and 1/6th or 1/7th power laws are the most popular way of extrapolating for velocity values outside the measured range of water column (Le Coz et al., 2012). Strictly speaking the log-profile is not supposed to describe the velocity distribution of the top 70 to 80 % of the water column (Nezu and Nakagawa, 1993). Power law profiles are mere approximations with little physical grounds. The information entropy (Shannon, 1948; Jaynes, 1957) provides an interesting alternative.

The maximization of the entropy (Jaynes, 1957) ensures that the probability distribution assigned to a series of values of a random variable subject to physical constraints, is the least biased (Jaynes, 2003). By information entropy theory, velocity profiles are derived by maximizing the entropy that depends on three parameters, the surface velocity u_s and two Lagrange multipliers in the case of two integral constraints (Chiu, 1987; Singh, 2014). The surface boundary condition imposes a relationship between these three parameters. Chiu (1987) showed that 1D vertical profiles derived from the information entropy theory match very closely the measured profiles, a result verified and refined by many later studies (Luo et al., 2018; Yeganeh and Heidari, 2020). As explained by Chiu (1987) fitted entropy-based profiles can be connected to log profile characteristics and especially used to determine the friction velocity. The study by Chiu (1987) has triggered a large amount of investigation using information entropy.

Information entropy theory can also be applied to describe 2D velocity distributions in a cross-section of a river Chiu (1988); Singh (2014). Because of the geometric extra degree of freedom compared to 1D cases, entropy based 2D distributions theories resort to assumptions on the shape of the isovel pattern in the cross-section (Chiu, 1988; Moramarco et al., 2004, 2017, 2019). These assumed isovel distributions have been thoroughly validated (Marini et al., 2017). This opens the way to discharge evaluations without any prior bathymetry surveys. Very recently such approach was effectively rendered operational by Moramarco et al. (2019) using developments of Moramarco et al. (2004) in such a way that allows discharge evaluations using satellite data such surface water velocity and elevation.

Entropy maximization yields a widely used relation between u_{max} and the cross-sectional average velocity U (Chiu, 1988, 1991; Chiu and Said, 1995),

$$U = u_{max}\,\Phi(M) \tag{1}$$

where Φ is a uniquely defined function and M the so-called entropy parameter. Empirical observations (Chiu and Said, 1995; Chen and Chiu, 2004; Moramarco et al., 2004; Chiu and Hsu, 2006; Fulton and Ostrowski, 2008; Ardiclioglu et al., 2012; Moramarco and Singh, 2010; Moramarco et al., 2017) show that M only depends on the river cross-section and thus that equation (1) is a one-to-one relation. In 2D distributions the maximum velocity does not necessarily occur at the free surface, a characteristic known as the dip phenomenon (Moramarco et al., 2017). This implies that discharge estimations based on (1) require exploring the velocity distribution within the flow area to determine u_{max}, an exploration only accessible to sophisticated methods such as aDcp's. Moreover, (1) implicitly allows for only one local maximum u_{max} in the cross-section which is not necessarily the case in river sections downstream of bends and meanders or with secondary currents. More generally it is reasonable to presume that because of the 3D nature of the flow with the complex distribution of secondary currents and the river geometry, the isovel patterns parametrization as given by Chiu (1988); Kumbhakar et al. (2019) is too schematic even though, as indicated previously, it is relevant for ungaged rivers (Moramarco et al., 2019). Therefore, in the present study we re-analyze 1D entropy-based distributions for video-based discharge estimations in regularly gaged rivers.

In section 2, the standard 1D information entropy theory is recalled. We show that it yields a relationship between surface velocity measurements and velocity vertical profiles characteristics allowing for easy discharge evaluations. Section 3 describes the gaging station were aDcp, surface imaging and stage data are acquired and at which a longstanding rating curve is available for our method validation. Section 4 discusses how reliable the sole use of video-based surface velocities is for discharge estimations. We conclude in Section 5.

2. Information entropy theory & discharge evaluations

For 1D vertical profiles, the time average stream-wise velocity u is assumed to be a random variable with a probability density function denoted $p(u)$. The Principle of Maximum Entropy (POME) is used to find the best fit distribution of velocity by maximizing the entropy of $p(u)$ subject to the basic constraints. Information entropy (Shannon, 1948; Jaynes, 1957; Chiu, 1987, 1988) which is a measure of the average information content in a set of observed velocity values u, is expressed as

$$H = -\int p(u)\,\ln(p(u))\,\mathrm{d}u \tag{2}$$

where $p(u)$ is the probability density function of the velocity values and the integral taken over all possible values of u. Definition (2) is referred to as the Shannon entropy. Other definitions such as the Tsallis or Renyi entropies are also used to define and approximate velocity distributions (Yeganeh and Heidari, 2020). The function $p(u)$ is by definition related to $F(u)$, the cumulative distribution function (CDF), in the following way,

$$F(u) = \text{probability that (velocity} \leq u) \tag{3}$$

$$p(u) = \frac{\mathrm{d}F}{\mathrm{d}u} \tag{4}$$

The probability density function $p(u)$ is subject to the following constraints (Chiu, 1987, 1988),

$$\int_0^{u_{max}} p(u)\,\mathrm{d}u = 1 \tag{5}$$

$$\int_0^{u_{max}} u\,p(u)\,\mathrm{d}u = \overline{u} \tag{6}$$

where u_{max} is the maximum velocity value, $\overline{u}$ the expected velocity. In the case of 1D profiles in wide channels Marini and Fontana (2020) showed that $\overline{u}$ is same as U, the vertical average. The Principle of Maximum Entropy (POME) (Chiu, 1987, 1988) involves not only (2) but also two Lagrange multipliers λ_1 and λ_2 associated to (5) and (6). Details of the calculus of variations are in Chiu (1987, 1988). It yields,

$$p(u) = e^{\lambda_0}\,e^{\lambda_2 u} \tag{7}$$

$$\lambda_0 = \lambda_1 - 1 \tag{8}$$

Obtaining the velocity distribution u requires some assumption on $p(u)$. In this paper, we focus on 1D distributions or said differently to rivers/channels wide compared to the water depth

(Chiu and Hsu, 2006). To that end Chiu (1987) assumed a monotonously increasing vertical velocity profile from bottom to the free surface. Thus $F(u)$ is the fraction of water column with all velocities smaller than u. This writes,

$$F(u(z)) = \frac{z}{D} \tag{9}$$

where D is the total water depth and $z = 0$ is the bottom. This form of CDF also implies that the maximum velocity u_{max} lies at the surface. The probability density function now writes,

$$p(u) = \frac{1}{D} \frac{\mathrm{d}z}{\mathrm{d}u} \tag{10}$$

Equating (7) to (10), integrating once and applying the boundary condition,

$$u = 0 \quad \text{at} \quad z = 0 \tag{11}$$

gives the mean stream-wise velocity profile expression,

$$u = \frac{1}{\lambda_2} \ln\left[1 + \lambda_2 \, e^{\lambda_0} \, \frac{z}{D}\right] \tag{12}$$

where λ_2 is dimensionally the inverse of a velocity and is found to be positive in the experiments. Many authors (Chiu, 1987, 1988) fit measured vertical profiles of streamwise velocity with (12) by calibrating the two free parameters λ_2 and λ_0. An alternate expression of u stems from the boundary condition,

$$u = u_s \quad \text{at} \quad z = D \tag{13}$$

or equivalently from (5) that gives a relationship between λ_2 and λ_0 that involves the surface velocity u_s of the profile,

$$\lambda_0 = \ln \lambda_2 - \ln\left(e^{\lambda_2 u_s} - 1\right) \tag{14}$$

and the following mean velocity profile expression,

$$u = \frac{1}{\lambda_2} \ln\left[1 + \left(e^{\lambda_2 u_s} - 1\right) \frac{z}{D}\right] \tag{15}$$

The key idea of the present study is to only use surface velocity measurements combined with the cross-section bathymetry to evaluate the discharge of large streams. In a wide channel (top width larger than depth), lateral bank friction has little influence on the isovel pattern. Isovels are nearly horizontal with therefore monotonously increasing velocities from bottom to free surface. Thus, each vertical profile can be advantageously fitted by a 1D velocity profile such as (12). The sole knowledge of u_s is not sufficient to compute the discharge with (15), the value of the Lagrange multiplier λ_2 is necessary. The extra assumption we introduce stems from an empirical observation by Singh (2014) in the case of 2D distributions that indicates a linear relationship between the two Lagrange multipliers. We assume that it is also true in 1D distributions and this will be verified in the course of this work. Therefore, we hypothesize that for a given water level or equivalently a given discharge, λ_0 and λ_2 for all verticals are linearly related. The rate of change of λ_0 with λ_2 derived from (14) writes,

$$m = \frac{\partial \lambda_0}{\partial \lambda_2} = \frac{1}{\lambda_2} - \frac{u_s \, e^{\lambda_2 \, u_s}}{e^{\lambda_2 \, u_s} - 1} \tag{16}$$

In situations where $\lambda_2 \, u_s$ is large, such as in the case of wide streams, this relation rewrites as,

$$\lambda_2 = \frac{1}{m + u_s} \tag{17}$$

This last relation will enter the following protocol. Vertical profiles of the horizontal velocity measured by aDcp, complemented with video surface velocities measurements, are approximated with (12) by calibrating λ_2 and λ_0. This provides a set of quasi-straight lines (Singh, 2014), parametrized by u_s the surface velocity. These lines will be linearly fitted to yield a calibrated m, which is nothing else than rating the m values with u_s. Once this rating is robust enough, any surface velocity measurement u_s can be associated to a m value. By (17) u_s and m are then used to compute λ_2 which in turn allows the evaluation of the unitary discharge q at the given X cross-wise location. An analytical expression of the unitary discharge q is easily computed from (15) by simple integration,

$$q(X) = \int_0^{D(X)} u \, \mathrm{d}z = \frac{D(X)}{\lambda_2} \frac{1}{e^{\lambda_2 \, u_s} - 1} \left[1 + (e^{\lambda_2 \, u_s} - 1) \, (\lambda_2 \, u_s - 1) \right] \tag{18}$$

Using formula (18) to compute q requires the knowledge of $D(X)$ the water depth at the different cross wise locations. Once the set of cross wise $q(X)$ values is computed, a numerical integration from the left bank X to the right bank X yields the total discharge Q.

3. Case study and available measurements

The Isère-Campus gaging station is located on the banks of the Isère River, a few kilometers upstream of Grenoble (France) on the main campus of the University of Grenoble-Alpes. Figure 1 shows an upstream bend and a bridge (130 m upstream of the gaging station). The bridge has no pier in the river thus generating no perturbations at the gaging station. The river bottom slope is $S_0 = 0.5 \, 10^{-3}$. The inter-annual average discharge of the Isère at Grenoble is $179.0 \, \mathrm{m}^3/\mathrm{s}$. The station is equipped for measuring and exploring river discharge, water level, water temperature, turbidity, concentration of suspended solids, and the velocity fields.

An unmanned vessel-mounted acoustic Doppler current profiler (aDcp; Nortek Rio Grande, 1200 kHz operated with WIN-RIVER II) collected velocity profiles of the entire channel to calculate channel velocities and discharge. The vessel is attached to a cable-way system spanning over the transect of the Isère river at the station. The cable-way system tows the vessel at the free surface across the transect. The aDcp sensors are located 0.1 m below the water surface. The aDcp has a blanking distance of 0.5 m, resulting in a measurement range from approximately 0.6 m below the water surface down to the top of the blanking zone near the river bottom. The blanking zone at the bottom is 0.6 m. Velocity data were collected at vertical cells of 0.10 m to 0.20 m in size at a frequency of roughly 1 Hz. In the present study two methods were used for the velocity profiles and discharge. One called continuous crossing method implied towing the aDcp across the river at nearly constant speed of roughly 0.18 m/s and the other called fixed vertical method for which the aDcp was stationary at a discrete and finite number of locations in the transect. The bottom-tracking mode of the aDcp was enabled both for the continuous crossings and fixed verticals. For the fixed vertical method, roughly 100 vertical profiles were recorded at each cross-wise position. In this case the discharge is computed with the midsection method. The panel assigned to a vertical is in that case centered on the vertical with left and right limits are midway from the adjacent verticals.

Figure 1: Top view and location (red point) of the Isère-Campus gaging station. Aerial image obtained from Imagery @2018 Google. The width of the river is roughly 60 m at the gaging station.

The station is also equipped with a staff gage installed on the left bank side to measure the stage (water level) H with a resolution of 1 cm. This stage measure is used in conjunction with a discharge rating curve Q_{RC}. The rating curve is a best fit power law based on discharge and stage measurements done at the Isère-Campus station between 1992 and 2018.

Table 1 provides an overview of all the experiments used in this work, including the deployed instruments. The bottom-tracking of the aDcp was used to determine the average cross-section bathymetry which is necessary for the discharge computation by the entropy method (see eq.18). Different types of measurements were combined to this end. The bathymetric surveys of the 5 continuous crossings for $H = 0.8$ m are averaged. This low discharge case does not allow for the higher parts of the bathymetry to be measured. To overcome this, the $H = 2.04$ m fixed vertical survey is used. The resulting average bathymetry is given in Figure 2. The cross-section shape is close to triangular. The right bank has a mild slope due to an alternate gravel bank whereas the right bank is steeper.

A video surveillance camera AXIS P1357-E (5 megapixels, 12 frames per second) was installed on the left bank. In order to reduce the transmission bandwidth and enable the real-time processing on a remote server (cloud computing), a burst of 4 images separated by 80 ms (median value) is sent by the camera to an FTP server. The camera was calibrated by the topographical survey of ground reference points visible in the camera image.

Over a region of 20 meters around the surveyed profile, the surface velocity vector field is

date	H (m)	aDcp method		surface velocity measure-ments	rating curve discharge Q_{RC} ($\mathrm{m^3/s}$)
		number of fixed verticals	number of continuous crossings		
18/10/2017	0.8	9	5	no	61.16
07/12/2015	1.275	none	4	no	105.72
01/12/2016	1.83	16	6	no	171.34
19/03/2018	2.04	20	none	yes	198.37
04/05/2018	2.92	none	6	yes	320.72
24/04/2018	3.02	none	8	yes	335.35
11/06/2018	3.39	27	none	yes	390.3
23/01/2018	4.05	none	6	yes	491.57
05/01/2018	5.18	none	none	yes	674.9

Table 1: Conditions and parameters of the different surveys. The stage reading is H.

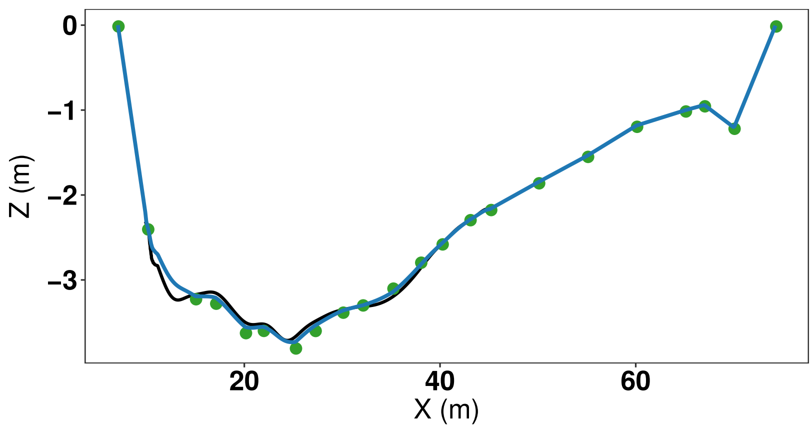

Figure 2: Cross section bottom profile at the Isère-Campus gaging station. Green dots: fixed vertical measurements for $H = 2.04$ m; black line: average bottom bathymetry of the 5 continuous crossings for $H = 0.8$ m; blue curve: average of these two bathymetries. The X axis is along the transect. $Z = 0$ corresponds to the free surface level for the stage $H = 2.04$ m.

measured by a PTV algorithm between successive images. The spatial resolution of this measured field is below 1 m. A consolidated vector field is then obtained for each burst of 4 images (Figure 3-a). A smoothing approach is used for the estimation of the streamwise surface velocity profile. The surface velocity field of Figure 3-a is projected and interpolated on the cross wise transect (see Figure 4 and Figure 3-b). The profile is extrapolated to the banks using the conservation of the Froude number hypothesis (Fulford and Sauer, 1986). This is useful for surface velocities far from the camera and especially close to the right bank. The median value of the proportion of extrapolated surface velocity profile is approximately 5 %. The velocity accuracy depends on the location on the profile (i.e. more dispersion on the right river bank), on the wa-

a)

b)

Figure 3: Surface fluid velocities extracted from surface video images on the 23/01/2018 for a stage of $H = 4.03$ m. a): raw PTV surface velocity vectors; b): estimated streamwise velocity profile. Color-bars are on the left of the images. River flowing from right to left and camera on the left bank.

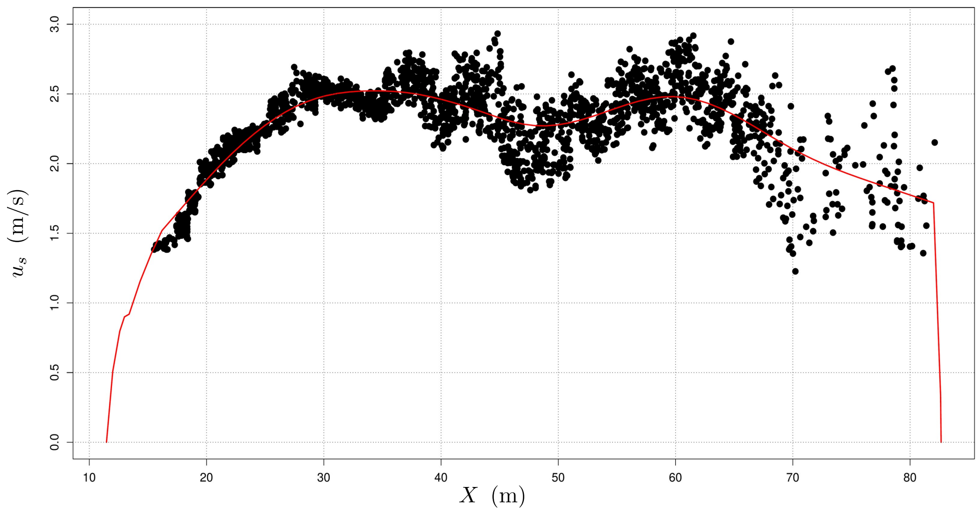

Figure 4: Surface velocity field u_s projected and interpolated on the surveyed cross section same date as in Figure 3 (23/01/2018) for a stage of $H = 4.03$ m. X: cross-wise coordinate. Black dots: velocity values. Red curve: best fit and same curve as in Figure 3-b.

ter level and on the illumination conditions. Overall, the relative error on the average surface velocity is between 2 % and 15 %.

4. Application

Fitting a time average velocity vertical profile is the initial step in the rating procedure of m by u_s. The time averaging for the fixed vertical method is obvious since for each verticals, corresponding to a cross wise position X, the vessel is stationary for a few minutes while it samples a sufficient number of instantaneous velocity vertical distributions. In contrast, for the continuous crossing method the vessel is towed along the transect of the cross-section measuring more than 200 verticals with unreferenced positions with respect to X. In this case, it was decided to average bins of 15 adjacent verticals together and then interpolate the obtained averaged velocity vertical distributions on a given X grid. This bin averaging is deemed to be equivalent to a time averaging since the vessel speed towed by the cable-way is small (of order 0.18 m/s) compared to the sampling rate of the aDcp (1 Hz).

Examples of time averaged horizontal velocity distribution profiles are plotted in Figure 5. They correspond to different verticals at different distances to the left bank of the cross-section. The fitted entropy-based velocity distributions are computed by merging the aDcp measurements, the surface video-based velocities and a bottom velocity imposed at zero value. The highest number of measured values on each vertical are those of the aDcp, they therefore strongly constrain the approximation. Video-based surface velocities are slightly scattered with respect to the entropy-based velocity distribution. However, the addition of video surface velocity data for the fitting improves the entropy parameter estimations. Figure 6 shows that the scatter of λ_1 and λ_2 is significantly reduced by the incorporation of a surface velocity in the data used for the fitting. The relationship between λ_1 and λ_2 clearly benefits from this addition.

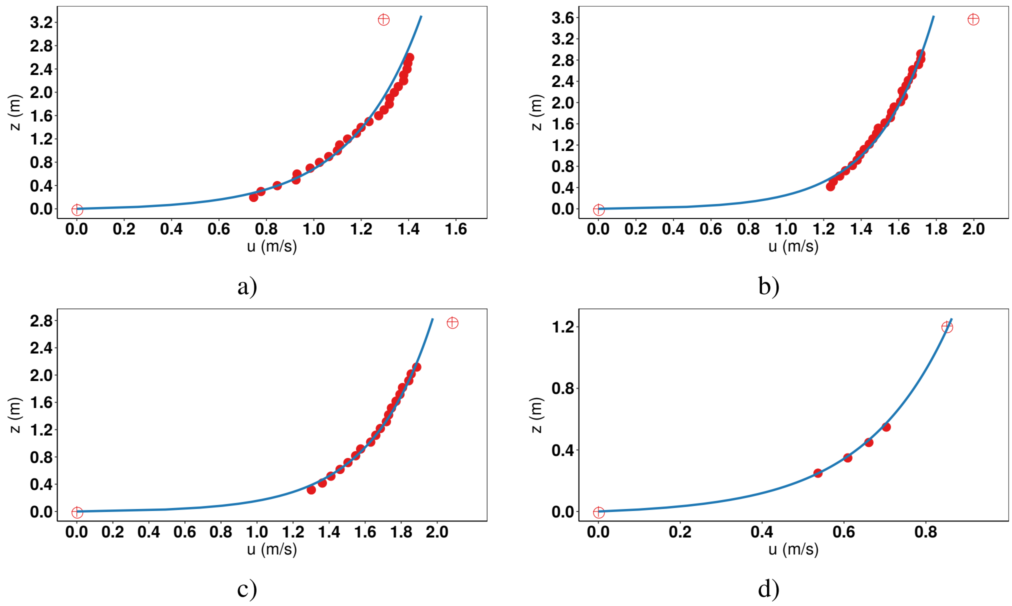

Figure 5: Calibration of entropy-based vertical velocity distributions. Stage $H = 2.04$ m case. a): $X = 17.07$ m; b): $X = 27.23$ m; c): $X = 38.02$ m; d): $X = 70.04$ m. Red dots: aDcp measurements. Top circle/cross point: video surface velocity. Bottom points at $z = 0$: circle/cross. Blue line: entropy-based velocity fitting. The z axis is the local vertical axis.

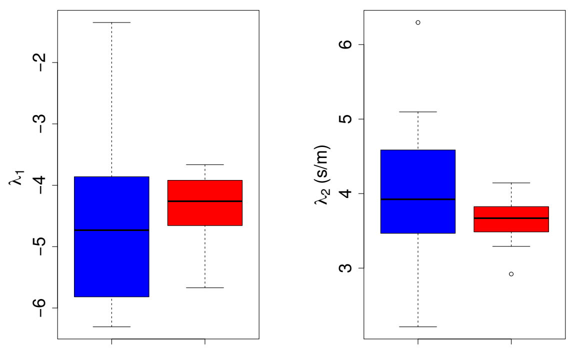

Figure 6: λ_1 and λ_2 boxplot distributions. blue boxplots: λ_1 and λ_2 determined with no video surface velocity incorporated in the fitting of (15); red boxplots : determined with video surface velocity incorporated in the fitting of (15). Stage at $H = 2.04$ m. Box: 2nd and 3rd quartile group; black line in the box: median value; whiskers: 1st and 4th quartile; dots: outliers

This entropy-based velocity distribution provides an extrapolation near the bed and below the surface in the blanking zones. It is interesting since the unitary discharge $q(X)$ is most sensitive to the near surface extrapolation because it corresponds to water layers with the highest velocities. A first check, summarized in Table 2, is undertaken to assess if entropy-fitted vertical profiles yield correct discharge estimates. On the one hand ("adcp" column of Table 2) $q(X)$ is estimated by a numerical integration by the trapezoidal rule of the vertical profile as given by the aDcp measurements with or without surface velocity estimations. On the other hand ("entropy" column of Table 2) $q(X)$ is computed by (18) for which λ_2 and u_s are provided for each vertical by the entropy fitting procedure. For both approaches the total discharge Q is given by the numerical integration bank to bank of the cross-wise $q(X)$ curve. Such procedure has been applied to 5 cases of Table 1 and the results are given in Table 2. The 5 cases where chosen so that the discharge increment between each estimations was roughly $100\,\mathrm{m^3/s}$ in order to cover regularly the range of discharges. The outcome is that the differences in discharge between the two approaches are small thus validating the use of entropy-based discharge estimate.

	Discharge ($\mathrm{m^3/s}$)		
H (m)	aDcp	entropy	diff. (%)
1.275	122.12	129.15	5.7
2.04	199.43	202.45	1.5
2.92	309.06	320.59	3.7
3.39	400.20	410.82	2.6
4.05	529.27	540.63	2.1

Table 2: Discharge computations. The stage is H. "aDcp" column: discharge computed by numerical integration of the data points with the adcp data and the video surface velocities when available (not measured for $H = 1.275\,\mathrm{m}$). "entropy" column: discharge computed with the cross-wise integration of (18). "Diff." column: difference in % between the two approaches.

The ultimate step is to understand and analyze if the discharge can be estimated just with video surface velocities. As discussed in section 2 we only have one theoretical relation (16) between λ_1 (or λ_0), λ_2 and u_s. So the sole use of surface velocities is conceivable if an extra relation between two of the three parameters of (16) is found. It happens that for a given stage, thus for a given maximum surface velocity, the pairs λ_1 and λ_2 at each vertical form a quasi-straight line as plotted in Figure 7. This was observed theoretically by Singh (2014) for 2D velocity distributions, and it is remarkable that the slope m of this relation is only a function of the surface maximum velocity U_{max}. This provides the empirical rating between m and the maximum surface velocity U_{max} we are looking for. Obviously, the more aDcp and surface velocity measurements are compiled, the more robust this relationship will be. Figure 8 shows that the relation between m and U_{max} is linear and thus, can be easily used to extrapolate for values outside the range of those already measured and especially at high discharges. Indeed in Figure 8 the lowest value corresponds to a discharge $Q = 61.16\,\mathrm{m^3/s}$ which is a very low value for the Isère since the inter-annual three days average minimum is roughly $80\,\mathrm{m^3/s}$. The slope m is negative thus for λ_2 to be positive, relation (17) says that $u_s > |m|$ which is the case as evidenced by Figure 8. The best fit line in Figure 8 is given by,

$$|m| = 0.774\, U_{max} - 0.0544 \quad \text{with} \;\; R^2 = 0.98 \tag{19}$$

The assumption of (17) is that $\lambda_2\, u_s$ is large. In Figure 9 the $\lambda_2\, u_s$ cross-wise distribution indicates that this quantity is in most positions above 5, a large enough value to make (17) valid. Indeed the function $e^\alpha / (e^\alpha - 1)$ in (16) is within 5 % of 1 for α above 3.

Finally the scheme to compute the discharge for a given stage H is the following:

1. video images are processed to supply a surface velocity profile $u_s(X)$;
2. the surface maximum U_{max} is extracted;
3. a unique m is determined by the "rating" curve of Figure 8 or equivalently with (19);

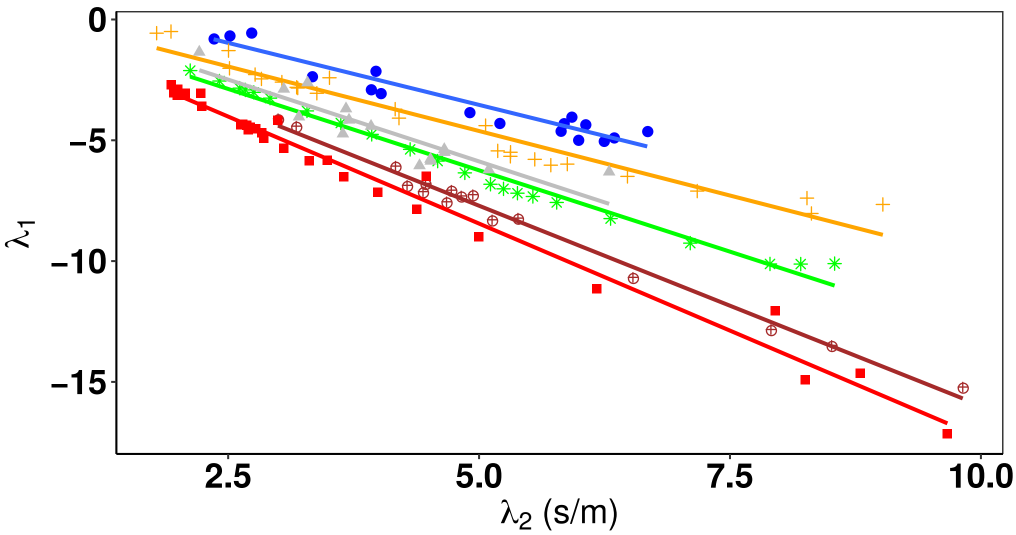

Figure 7: Experimental relationship of λ_2 with λ_1 for different stages. Color lines: best linear fit of the data (points) of same color. Blue: $H = 0.8$ m and $U_{max} = 1.31$ m/s; yellow: $H = 1.275$ m and $U_{max} = 1.53$ m/s; green: $H = 1.83$ m and $U_{max} = 1.79$ m/s; grey: $H = 2.04$ m and $U_{max} = 1.93$ m/s; brown: $H = 2.92$ m and $U_{max} = 2.17$ m/s; red: $H = 4.05$ m and $U_{max} = 2.42$ m/s.

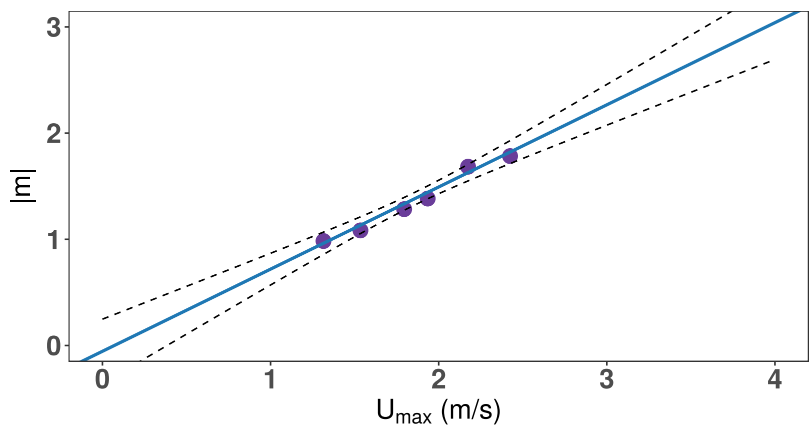

Figure 8: Relation between the module $|m|$ of the slope (16) and the surface maximum velocity U_{max}. Purple circles: data; blue plain line: best linear fit regression line; black dashed line: 95 % confidence interval.

4. relation (17) is used to determine $\lambda_2(X)$ at each X where a surface velocity is given;
5. $q(X)$ is computed by (18);
6. a bank to bank numerical integration of $q(X)$ supplies the total discharge $Q(H)$.

The scheme described above to determine Q using only video recorded surface velocities is now applied to three cases given in Table 3. For two of the cases m is not in the range of those of Figure 8. The one for $H = 5.18$ is for a flood situation. For each video surface velocity u_s along

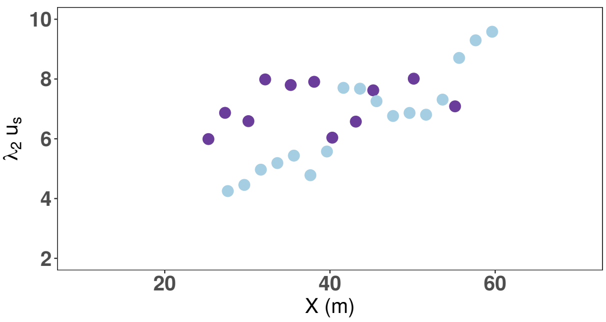

Figure 9: The $\lambda_2\, u_s$ cross-wise distribution. Purple: stage at $H = 2.04$ m; light blue: stage at $H = 4.05$ m.

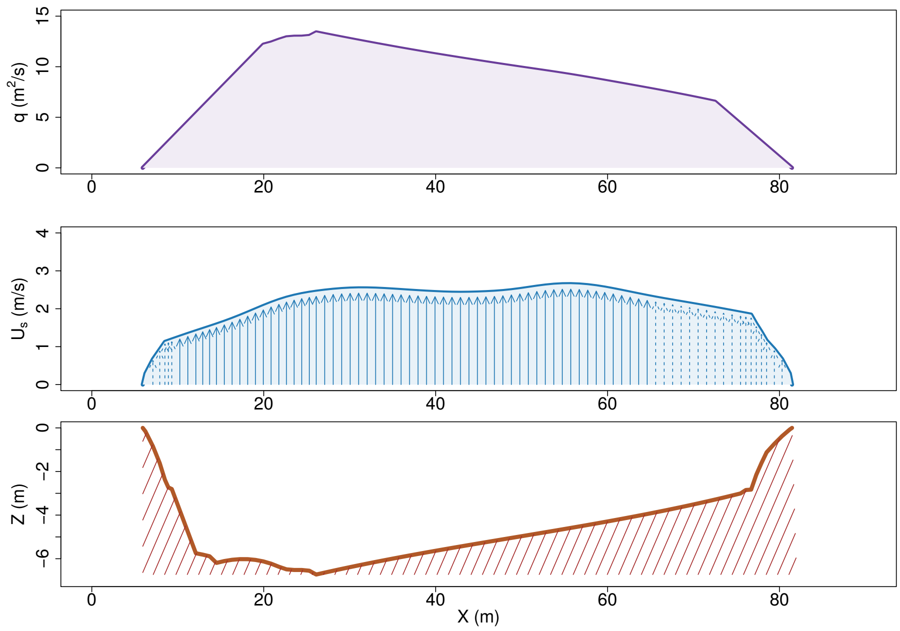

Figure 10: Case with stage at $H = 5.18$ m with no aDcp measurements. middle panel: interpolated measured video-based surface velocity u_s distribution; dashed vectors: extrapolated vectors. Top panel: cross-wise distribution of unitary discharge $q(X)$ by the full entropy method. Bottom panel: cross-section profile, $Z = 0$ corresponds to the free surface level.

the cross-wise transect λ_2 is computed by (17) using the unique m from (19). The q values along the transect are determined by (18). A example of the q crosswise profile is plotted in Figure 10 for the $H = 5.18$ case. In the Q column of Table 3 the upper bound and lower bound of Q as computed by the 95 % confidence interval on m of Figure 8 are given. Predicted values are all close to the rating curve value Q_{RC} of the discharge. The uncertainty interval contains the Q_{RC} value except for the $H = 1.66$ case which falls very close at 4 m^3/s from that interval. Recall that at this stage of our work, the confidence interval for the "rating" curve Figure 8 is based on only 6 points. The uncertainties will decrease by incorporating more measurements with time.

date	H (m)	U_{max} (m/s)	m	Q (m^3/s)	Q_{RC} (m^3/s)	error (%)
13/12/2017	1.66	1.58	-1.17	170.9 ± 17.3	151	13.2
24/04/2018	3.02	2.26	-1.69	348.8 ± 20.3	352	0.9
05/01/2018	5.18	2.64	-1.99	657.3 ± 44	674.9	2.6

Table 3: Video alone discharge evaluations. The stage is H; U_{max} is the maximum video measured surface velocity; Q the computed total discharge; Q_{RC} the rating curve discharge associated with H; error column is the relative difference between Q and Q_{RC}.

Noteworthy is the double maximum of the surface velocity in Figure 10 also appearing in Figure 4 for another stage. This may be due to the river bend roughly 300 meters upstream (Figure 1). Had we used the 2D entropy based velocity distribution the determination of the "y-axis" would have been uncertain.

5. Conclusions

In the present study, we have developed, calibrated and validated a novel approach for discharge estimations with image-based surface velocities. The method draws on information entropy derived 1D velocity distributions, applicable to rivers large compared to the water depth. The method once calibrated only requires surface stream-wise velocities such as those provided by video imaging. The calibration relies on the rating of the slope m of the relation between the two Lagrange multipliers λ_2 and λ_1 of the information entropy theory. The rating of m with the maximum surface stream-wise velocity is provided by conventional aDcp surveys of the cross-sectional velocity distribution and video-based surface velocities. These heterogeneous data sources describing different velocity vertical profiles are merged and approximated with theoretical 1D velocity distributions given by the information entropy theory. Our data confirms that λ_2 and λ_1 are indeed linearly related and that the calibration clearly benefits from the addition of measured surface velocities. The method applied to the Isère river at the Isère-Campus gaging station is totally consistent with the longstanding rating curve between stage and discharge of this gaging station. The deployment of aDcps with smaller blanking zones could improve the calibration by providing more information especially in the top layers of the water column. Furthermore, extra calibration data will be valuable to improve the m-U_{max} rating curve.

6. Acknowledgements

The first author is very grateful to TENEVIA for the internship grant they offered. We express our deepest gratitude to Christophe Rousseau for his continuous technical support. We are thankful to ENSE3 (Ecole Nationale Supérieure de l'Energie, l'Eau, et l'Environnement) and EDF-DTG (Electricité de France - Direction Technique Générale) for granting us access to the Isère-Campus gaging station.

References

Ardiclioglu, M., Genc, O., Kalin, L., Agiralioglu, N., 2012. Investigation of flow properties in natural streams using the entropy concept. Water and Environment Journal 26, 147–154.
Chen, Y.C., Chiu, C.L., 2004. A fast method of flood discharge estimation. Hydrological Processes 18, 1671–1684.

Cheng, N.S., 2007. Power-law index for velocity profiles in open channel flows. Advances in Water Resources 30, 1775 – 1784. doi:https://doi.org/10.1016/j.advwatres.2007.02.001.
Chiu, C.L., 1987. Entropy and probability concepts in hydraulics. Journal of Hydraulic Engineering 113, 583–600.
Chiu, C.L., 1988. Entropy and 2-d velocity in open channels. Journal of Hydraulic Engineering 114, 738–756.
Chiu, C.L., 1991. Application of entropy concept in open-channel flow study. Journal of Hydraulic Engineering 117, 615–628.
Chiu, C.L., Hsu, S.M., 2006. Probabilistic approach to modeling of velocity distributions in fluid flows. Journal of Hydrology 316, 28–42.
Chiu, C.L., Said, C., 1995. Maximum and mean velocities and entropy in open-channel flow. Journal of Hydraulic Engineering 121, 26–35.
Creutin, J., Muste, M., Bradley, A., Kim, S., Kruger, A., 2003. River gauging using piv techniques: a proof of concept experiment on the Iowa River. Journal of Hydrology 277, 182–194.
De Prony, G., 1804. Recherches physico-mathématiques sur la théorie du mouvement des eaux courantes. Imprimerie Impériale, Paris.
Dulos, P., 1877. Cours de mécanique à l'usage des Ecoles d'Arts et Métiers et de l'enseignement spécial des Lycées. Gauthier–Villard.
Fujita, I., 1997. Surface velocity measurement of river flow using video images of an oblique angle, in: Proceedings of the 27th Congress of IAHR, San Francisco, CA, pp. 227–232.
Fujita, I., Komura, S., 1994. Application of video image analysis for measurements of river surface flows. Proceedings of Hydraulic Engineering 38, 733–738.
Fujita, I., Notoya, Y., Tani, K., Tateguchi, S., 2019. Efficient and accurate estimation of water surface velocity in STIV. Environmental Fluid Mechanics 19, 1363–1378. doi:10.1007/s10652-018-9651-3.
Fujita, I., Watanabe, H., Tsubaki, R., 2007. Development of a non-intrusive and efficient flow monitoring technique: The space-time image velocimetry (stiv). International Journal of River Basin Management 5, 105–114.
Fulford, J., Sauer, V., 1986. Comparison of velocity interpolation methods for computing open-channel discharge. Water Supply Paper 2290. US Geological Survey. doi:10.3133/wsp2290.
Fulton, J., Ostrowski, J., 2008. Measuring real-time streamflow using emerging technologies: Radar, hydroacoustics, and the probability concept. Journal of Hydrology 357, 1–10.
Gunawan, B., Sun, X., Sterling, M., Shiono, K., Tsubaki, R., Rameshwaran, P., Knight, D., Chandler, J., Tang, X., Fujita, I., 2012. The application of LS-PIV to a small irregular river for inbank and overbank flows. Flow Measurement and Instrumentation 24, 1–12.
Jaynes, E., 1957. Information theory and statistical mechanics. Physical Review 106, 620–630.
Jaynes, E., 2003. Probability theory: The logic of science. Cambridge university press.
Kästner, K., Hoitink, A., Torfs, P., Vermeulen, B., Ningsih, N.S., Pramulya, M., 2018. Prerequisites for accurate monitoring of river discharge based on fixed-location velocity measurements. Water Resources Research 54, 1058–1076.
Kumbhakar, M., Ghoshal, K., Singh, V., 2019. Two-dimensional distribution of streamwise velocity in open channel flow using maximum entropy principle: Incorporation of additional constraints based on conservation laws. Computer Methods in Applied Mechanics and Engineering 361, 112738.
Le Coz, J., Camenen, B., Peyrard, X., Dramais, G., 2012. Uncertainty in open-channel discharges measured with the velocity-area method. Flow Measurement and Instrumentation 26, 18–29.
Le Coz, J., Hauet, A., Pierrefeu, G., Dramais, G., Camenen, B., 2010. Performance of image-based velocimetry (lspiv) applied to flash-flood discharge measurements in mediterranean rivers. Journal of hydrology 394, 42–52.
Luo, H., Singh, V., Schmidt, A., 2018. Comparative study of 1D entropy-based and conventional deterministic velocity distribution equations for open channel flows. Journal of Hydrology 563, 679–693.
Manfreda, S., Pizarro, A., Moramarco, T., Cimorelli, L., Pianese, D., Barbetta, S., 2020. Potential advantages of flow-area rating curves compared to classic stage-discharge-relations. Journal of Hydrology 585, 124752.
Marini, G., Fontana, N., 2020. Mean velocity and entropy in wide channel flows. Journal of Hydrologic Engineering 25, 06019009.
Marini, G., Fontana, N., Singh, V., 2017. Derivation of 2d velocity distribution in watercourses using entropy. Journal of Hydrologic Engineering 22, 04017003.
Moramarco, T., Barbetta, S., Bjerklie, D., Fulton, J., Tarpanelli, A., 2019. River bathymetry estimate and discharge assessment from remote sensing. Water Resources Research 55, 6692–6711.
Moramarco, T., Barbetta, S., Tarpanelli, A., 2017. From surface flow velocity measurements to discharge assessment by the entropy theory. Water 9, 120.
Moramarco, T., Saltalippi, C., Singh, V., 2004. Estimation of mean velocity in natural channels based on chiu's velocity distribution equation. Journal of Hydrologic Engineering 9, 42–50.
Moramarco, T., Singh, V., 2010. Formulation of the entropy parameter based on hydraulic and geometric characteristics of river cross sections. Journal of Hydrologic Engineering 15, 852–858.
Mueller, D., 2013. *extrap*: Software to assist the selection of extrapolation methods for moving-boat adcp streamflow

measurements. Computers & Geosciences 54, 211–218.
Muste, M., Fujita, I., Hauet, A., 2008. Large-scale particle image velocimetry for measurements in riverine environments. Water Resources Research 40.
Nezu, I., Nakagawa, H., 1993. Turbulence in open-channel flows, iahr monograph series. A.A. Balkema, Rotterdam , 1–281.
Perks, M., 2020. Klt-iv v1. 0: image velocimetry software for use with fixed and mobile platforms. Geoscientific Model Development 13, 6111–6130.
Rantz, S., 1982. Measurement and computation of streamflow. Water Supply Paper 2175. US Geological Survey. doi:10.3133/wsp2175.
Shannon, C., 1948. A mathematical theory of communication. The Bell System Technical Journal 27, 623–656.
Singh, V.P., 2014. Entropy Theory in Hydraulic Engineering: An Introduction. American Society of Civil Engineers.
Tauro, F., Piscopia, R., Grimaldi, S., 2019. PTV-Stream: A simplified particle tracking velocimetry framework for stream surface flow monitoring. CATENA 172, 378–386.
Yeganeh, M., Heidari, M., 2020. Estimation of one-dimensional velocity distribution by measuring velocity at two points. Flow Measurement and Instrumentation 73, 101737.